

# Phase-Variance Thresholding and Uncertainty-based Weighted Averaging for Optimal Generation of InSAR-derived Mosaics of Permafrost Active Layer Thickness

R. J. Michaelides, Department of Geophysics, EE 368 term project

## 1. Motivation

Large-scale thawing of arctic permafrost has a poorly-understood feedback effect on global climate through the release of CO<sub>2</sub> and methane. Active Layer Thickness (ALT) is the maximum annual depth of thaw of surface soils and is designated by the World Meteorological Organization (WMO) as an essential climate variable for monitoring the status of permafrost. Interferometric Synthetic Aperture Radar (InSAR) is a widely-used geophysical technique for measuring surface deformation at high spatial resolution (Rosen et al. 2000). In recent years, InSAR has been successfully used to measure ground deformation due to seasonal permafrost freeze/thaw cycles and invert this deformation signature for a spatially extensive and finely-sampled map of ALT (Liu et al. 2012; Schaefer et al. 2015).

## 2. Background

Interferometric synthetic aperture radar (InSAR) is a well-established radar remote sensing technique (Rosen et al. 2000). The synthetic aperture radar (SAR) technique utilizes the principle of coherent radar pulse integration, and doppler processing to generate high-resolution (~5-10 m pixel resolution) radar images of the earth's surface from earth-orbiting satellites (Rosen et al. 2000). When multiple SAR images over a single region of interested are acquired, the (element-wise) product of one image with the complex conjugate of the other image yields the difference in phase between these two images. Because this phase is directly related to distance, this image of phase differential (hereafter referred to as an interferogram), encapsulates information related to the earth's topography, and any surface deformation that occurred in-between the acquisition times of the two images (Rosen et al. 2000).

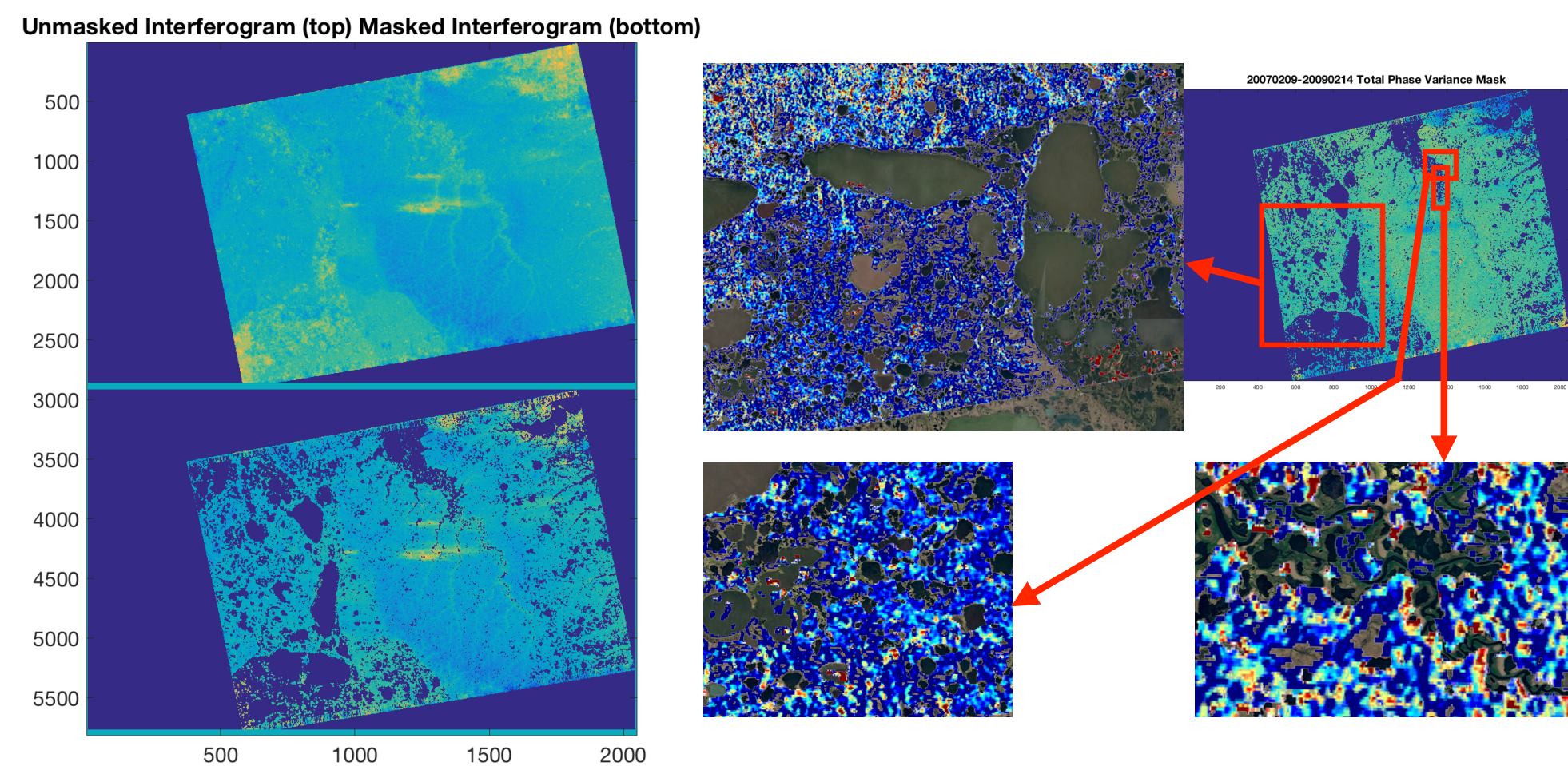


Figure 1: (Left) Interferogram unmasked (top) and masked with the phase-variance thresholding mask (bottom). (Right) Comparison of the mask's derived edges with surface optical imagery. The phase variance thresholding mask successfully masks out water regions, and preserves borders.

In recent years, the InSAR technique has been used to study the ground deformation associated with freeze/thaw surface subsidence in arctic permafrost environments. Permafrost environments are regions that are cold enough such that the groundwater held in the pore space of soils is completely frozen for a significant portion of the year. During the spring thaw period, rising surface temperatures cause pore space water to gradually thaw from solid to liquid; because a given amount of water takes more volume in its solid state than its liquid state, this phase change of water causes the ground to subside (or 'sink' downwards) due to the effective decrease in volume in a column of soil during thaw. As the spring season progresses through summer, extended periods of above-zero surface temperature cause more and more of the subsurface pore water to thaw, thereby causing a greater amount of subsidence. Eventually, a given region of permafrost will experience its maximum thaw during the thaw season; the depth to which the subsurface has thawed is referred to as the active layer thickness (ALT). In autumn and winter, this liquid water freezes again, and the ground experiences uplift (or 'rises' upward) as the effective volume of the pore space in a soil column increases. Thus, over a seasonal cycle, permafrost environments experience freeze/thaw-associated cycles of ground deformation, which can be imaged and characterized by InSAR.

## 3. Phase-Variance Threshold Masking

Arctic wetland regions of discontinuous permafrost are dotted with surface water features (lakes, thaw ponds, rivers, marshes, etc). Due to the scattering interaction of radar pulses and these water surfaces, phase estimates from these surfaces are unreliable in interferograms, and can therefore bias estimates of ALT, and must be masked out for optimal ALT distribution reconstructions. To address this, I have implemented a thresholding masking routine that utilizes phase variance as a threshold. The phase-variance masking routine takes advantage of the scattering interaction of radar pulses with water surfaces to directly identify regions within an interferogram that are water surfaces (without the use of secondary information such as optical imagery), and then mask out these regions.

The phase variance of each interferogram in a stack is calculated. For a stack of N interferograms, an image of normalized phase variance is generated by summing the normalized difference of a threshold phase variance and the per-pixel interferogram variance. After summation, a threshold value of zero is chosen, and all pixels in the normalized phase variance image exhibiting a value greater than zero are set to 1, while all values of zero are kept at zero. Thus, this mask removes all pixels that consistently exhibit a phase variance greater than the threshold phase variance across all N interferograms.

$$M_{i,j} = 1, \text{ if } V_{i,j} > 0$$

$$M_{i,j} = 0, \text{ if } V_{i,j} = 0$$

$$V_{i,j} = \sum_{k=1}^N \left( 1 - \left( \frac{\sigma_{k,i,j}}{\sigma_{threshold}} \right) \right)$$

$$E_{i,j} = \frac{\sum_{k=1}^{N_o} \frac{I_{k,i,j}}{(\sigma_{k,i,j})^2}}{\sum_{k=1}^{N_o} (\sigma_{k,i,j})^2}$$

No = Number of overlapping images per pixel  
I<sub>k,i,j</sub> = pixel (i,j) of the kth image I

## Unmasked ALT (top) and Masked ALT (bottom)

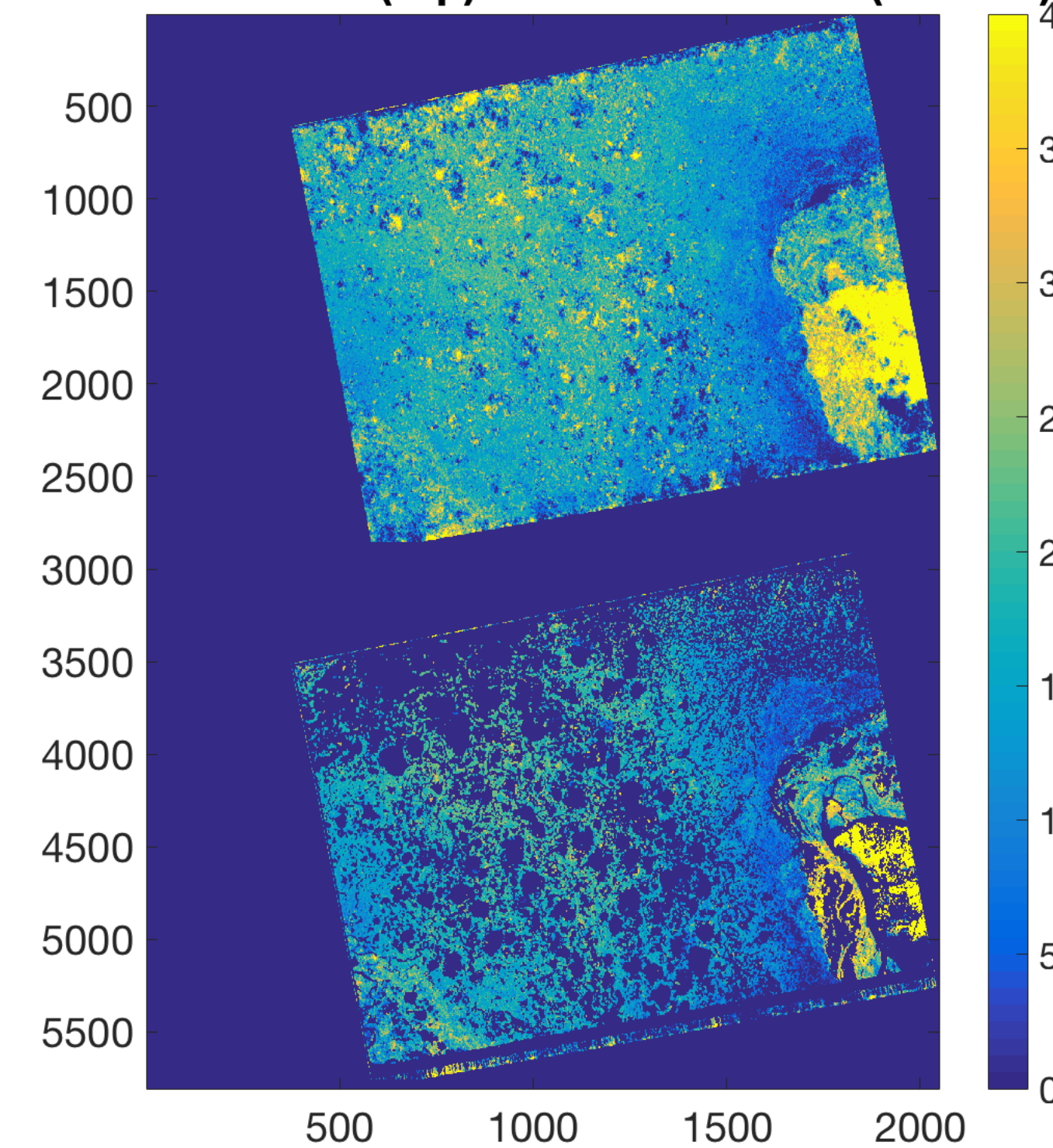


Figure 2: (Top) ALT distribution unmasked (top) and masked using the phase variance threshold mask (bottom). Notice that the mask successfully removes anomalous, unphysical large estimates of ALT that occur at the surface of thaw ponds (bright yellow at top, masked out at bottom).

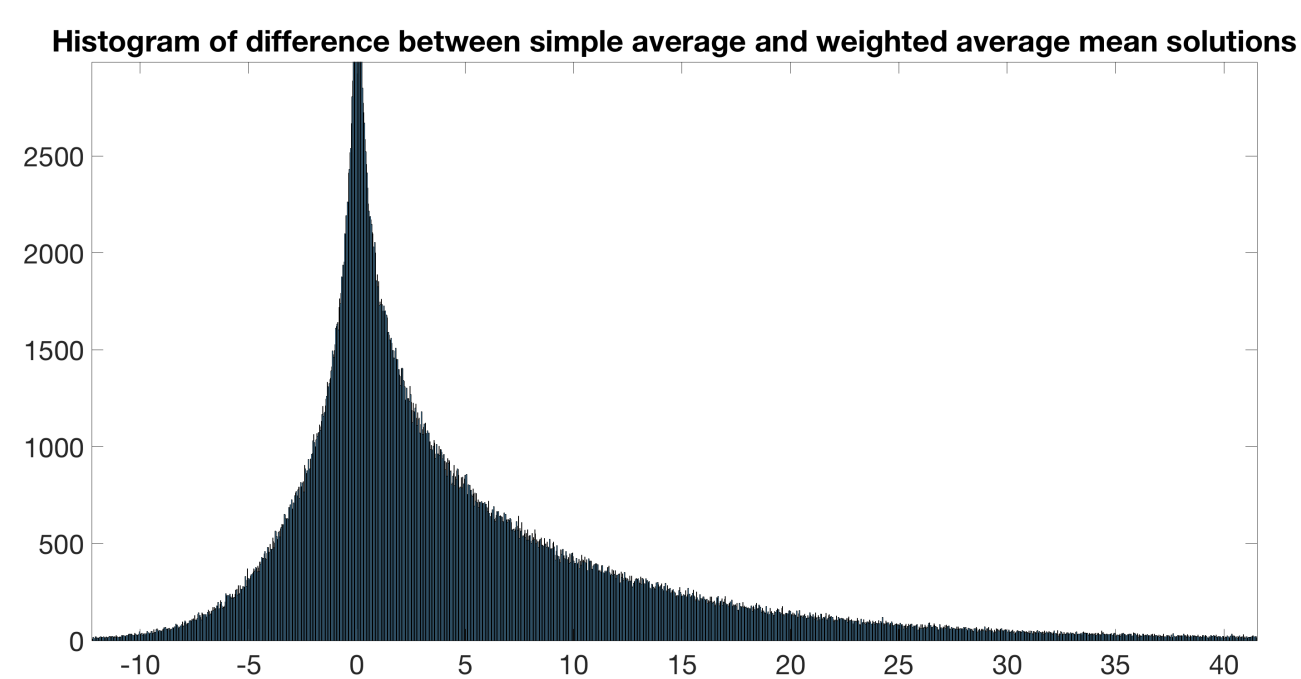
## 4. Weighted Arithmetic Mean Mosaicking

I have developed a weighted arithmetic mean mosaicking algorithm that can be used to stitch together several scenes of estimated ALT, so that larger regional maps of ALT can be generated. Instead of using a conventional mosaicking technique (such as feathering), I wanted to implement a method that took into account the uncertainties in measured ALT as a weighting method, so that ideally the mosaicking algorithm did not bias the measured values of ALT.

The weighted arithmetic mean mosaicking algorithm I developed utilizes the ALT and ALT uncertainty images for each stack, as well as their associated latitude and longitude ranges as inputs. The algorithm first determines the spatial offsets between each image, and generates a global scene within which it places each image. Then, the algorithm determines the regions of overlap between all of the images, and performs a weighted arithmetic mean of each overlapping image, using the ALT image's associated uncertainties as its weighting term.

The output mosaic is compared to mosaics generated with a simple averaging technique. The weighted arithmetic mean is seen to produce 'smoother' distributions of ALT when compared to these simpler mosaicking routines. Furthermore, by incorporating actual uncertainty measurements into the estimate, this averaging routine does not introduce artificial biases into the physical ALT estimate in regions of image overlap.

Figure 3: (Below) Histogram of values for the difference between the simple average mosaic and weighted arithmetic mean mosaic. Most values are centered at zero (pixels with no overlap between images), but significant deviations between the two methods occur for regions of image overlap.



## Weighted Average Mean Mosaic of 4 ALT Scenes

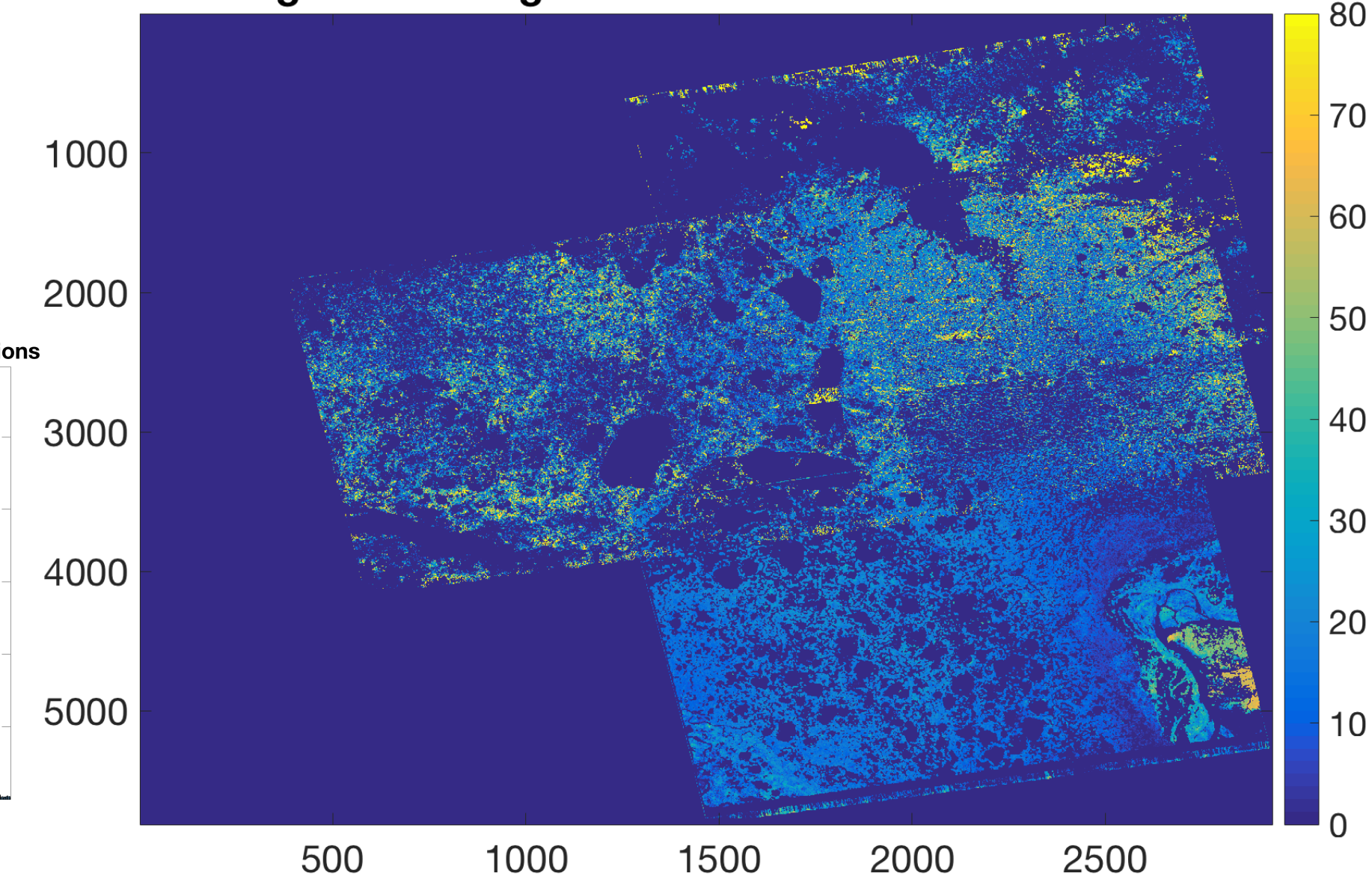


Figure 4: Georeferenced global mosaic of 4 separate images of ALT distribution. Images are coregistered using their respective geographic information from SAR processing, and are mosaicked together with the weighted arithmetic mean algorithm. This technique 'blends' along the discontinuous edges of each image, while keeping ALT estimates physically realistic by using the associated pixel uncertainty values as the weighting elements.

## 5. References

Rosen P. A. et al. 2000 Proc. IEEE, vol. 88, no. 3.; Schaefer, K. et al. 2015 Remote Sens. vol. 7, 2015.; Liu, L. et al. 2012 J. Geophys. Res vol. 117.